IJMMM International Journal of Minerals, Metallurgy and Materials 矿物冶金与材料学报（英文版）

Preparation of high-purity fluorite and nanoscale calcium carbonate from low-grade fluorite

Qianqian Lu, Haisheng Han, Wenjuan Sun, Xingfei Zhang, Weiwei Wang, Bilan Zhang, Wensheng Chen, and Qin Zou

Cite this article as:
Qianqian Lu, Haisheng Han, Wenjuan Sun, Xingfei Zhang, Weiwei Wang, Bilan Zhang, Wensheng Chen, and Qin Zou, Preparation of high-purity fluorite and nanoscale calcium carbonate from low-grade fluorite, *Int. J. Miner. Metall. Mater.*, 31(2024), No. 6, pp. 1198-1207. https://doi.org/10.1007/s12613-023-2697-3

Articles you may be interested in

Tian-yang Hu, Ti-chang Sun, Jue Kou, Chao Geng, and Yong-qiang Zhao, Effects and mechanisms of fluorite on the co-reduction of blast furnace dust and seaside titanomagnetite, *Int. J. Miner. Metall. Mater.*, 24(2017), No. 11, pp. 1201-1210. https://doi.org/10.1007/s12613-017-1512-4

Zulfiadi Zulhan and Windu Shalat, Evolution of ferronickel particles during the reduction of low-grade saprolitic laterite nickel ore by coal in the temperature range of 900–1250°C with the addition of CaO–CaF_2–H_3BO_3, *Int. J. Miner. Metall. Mater.*, 28(2021), No. 4, pp. 612-620. https://doi.org/10.1007/s12613-020-2025-0

Jing-cheng Wang, Lei Li, and Yong Yu, Tin recovery from a low-grade tin middling with high Si content and low Fe content by reduction–sulfurization roasting with anthracite coal, *Int. J. Miner. Metall. Mater.*, 28(2021), No. 2, pp. 210-220. https://doi.org/10.1007/s12613-020-2038-8

Jon Derek Loftis and Tarek M. Abdel-Fattah, Nanoscale electropolishing of high-purity nickel with an ionic liquid, *Int. J. Miner. Metall. Mater.*, 26(2019), No. 5, pp. 649-656. https://doi.org/10.1007/s12613-019-1773-1

Xu-zhong Gong, Jun-qiang Zhang, Zhi Wang, Dong Wang, Jun-hao Liu, Xiao-dong Jing, Guo-yu Qian, and Chuan Wang, Development of calcium coke for CaC_2 production using calcium carbide slag and coking coal, *Int. J. Miner. Metall. Mater.*, 28(2021), No. 1, pp. 76-87. https://doi.org/10.1007/s12613-020-2049-5

Feng Li, Qing-jie Zhao, Man-sheng Chu, Jue Tang, Zheng-gen Liu, Jia-xin Wang, and Sheng-kang Li, Preparing high-purity iron by direct reductionsmelting separation of ultra-high-grade iron concentrate, *Int. J. Miner. Metall. Mater.*, 27(2020), No. 4, pp. 454-462. https://doi.org/10.1007/s12613-019-1959-6

IJMMM WeChat

QQ author group

INTERNATIONAL JOURNAL OF
Minerals, Metallurgy and Materials

Volume 31, Number 6, June 2024
Page 1198

Research Article https://doi.org/10.1007/s12613-023-2697-3

Preparation of high-purity fluorite and nanoscale calcium carbonate from low-grade fluorite

Qianqian Lu[1)], *Haisheng Han*[1),✉], *Wenjuan Sun*[1)], *Xingfei Zhang*[1)], *Weiwei Wang*[3),✉], *Bilan Zhang*[4)], *Wensheng Chen*[2)], *and Qin Zou*[4)]

1) School of Minerals Processing and Bioengineering, Central South University, Changsha 410083, China
2) Hunan Nonferrous Chenzhou Fluoride Chemical Co., Ltd., Chenzhou 423000, China
3) State Key Laboratory of Baiyunobo Rare Earth Resource Researches and Comprehensive Utilization, Baotou Research Institute of Rare Earths, Baotou 014030, China
4) Hunan Shizhuyuan Nonferrous Metal Co., Ltd., Chenzhou 423000, China
(Received: 24 March 2023; revised: 25 June 2023; accepted: 27 June 2023)

Abstract: Flotation separation of calcite from fluorite is a challenge on low-grade fluorite flotation that limits the recovery and purity of fluorite concentrate. A new acid leaching–flotation process for fluorite is proposed in this work. This innovative process raised the fluorite's grade to 97.26wt% while producing nanoscale calcium carbonate from its leachate, which contained plenty of calcium ions. On the production of nanoscale calcium carbonate, the impacts of concentration, temperature, and titration rate were examined. By modifying the process conditions and utilizing crystal conditioning agents, calcite-type and amorphous calcium carbonates with corresponding particle sizes of 1.823 and 1.511 μm were produced. The influence of the impurity ions Mn^{2+}, Mg^{2+}, and Fe^{3+} was demonstrated to reduce the particle size of nanoscale calcium carbonate and make crystal shape easier to manage in the fluorite leach solution system compared with the calcium chloride solution. The combination of the acid leaching–flotation process and the nanoscale calcium carbonate preparation method improved the grade of fluorite while recovering calcite resources, thus presenting a novel idea for the effective and clean usage of low-quality fluorite resources with embedded microfine particles.

Keywords: fluorite; calcite; nanoscale calcium carbonate; waste recovery

1. Introduction

Fluorite is the most important raw material in the fluorine industry. It is widely used in traditional industries (e.g., metallurgy, construction, and chemicals) and strategic new industries (e.g., optics, medicine, and new energy) and is of great significance to the development of the national economy [1–6]. Fluorite can be divided into three grades: acid, ceramic, and metallurgical. Fluorite with a metallurgical grade of 65wt%–85wt% is mainly used in iron and steel smelting to lower the metal melting point. Meanwhile, fluorite with a ceramic grade is 85wt%–95wt% is used to promote the sintering of ceramics and improve the quality of porcelain glaze, while fluorite with a 97wt% acid grade is commonly used to react with sulfuric acid to produce hydrofluoric acid [7]. As the demand for fluorspar resources grows and single fluorite minerals are depleted, complex and hard-to-sort fluorite minerals are gaining traction. Most fluorite deposits are syngenetic minerals, which can be mainly divided into quartz-type, calcite-type, barite-type, and polymetallic symbiosis-type [8–9]. Given that calcite is the main associated mineral [10], therefore, the efficient separation of fluorite and calcite is the key to unlocking and exploiting these resources. Fluorite and calcite are both calcium-containing minerals with close floatability, and it is difficult to achieve efficient separation by traditional beneficiation methods, especially for calcite-type fluorite with fine chimeric particle size and complex symbiosis [10–12].

Recent research has shown that acid leaching can separate calcite particles that are difficult to separate from fluorite by conventional flotation methods and further dissociate other gangue particles to efficiently improve the grade of refractory fluorite [13]. However, the high cost is one of the main reasons that has limited the application of the acid leaching process. In addition, the calcium leaching solution produced during the acid leaching process proved to be a challenging material for the beneficiation plants. Using acid leaching waste to prepare high-value-added products is an effective solution to this problem, bringing additional economic benefits by reducing the cost of acid leaching and solving the problem of treating waste while maintaining the efficiency of the processing plant to protect the environment and save resources. El-Sheikh and Rabah [14] synthesized calcium chromate one-dimensional (1D) rods from tannery waste solution.

✉ Corresponding authors: Haisheng Han E-mail: hanhai5086@csu.edu.cn; Weiwei Wang E-mail: viviw91@163.com

Luo *et al*. [15] studied the synthesis of calcium carbonate from the waste liquid of ammonia evaporation, while Korkut *et al*. [16] used waste liquid from the synthetic soda ash industry to produce calcium carbonate, which is the most used high-value-added product.

Nanoscale calcium carbonate is widely used in papermaking [17], the plastics industry [18], the construction industry [19], coating [20], the materials industry [21], environmental protection [22], medicine [23], batteries [24], and other industries. The preparation of calcium carbonate with chemical methods is divided into carbonization, double decomposition, and biomineralization [25–27]. The crystalline forms of calcium carbonate include amorphous, aragonite, vaterite, and calcite. In recent years, many studies have focused on the preparation of nanometer calcium carbonate with a single crystal, and small particle size has always been the focus of calcium carbonate studies. The crystal type and size of calcium carbonate are affected by process conditions, such as concentration, temperature, rate, and crystal regulator [28–31], the pH and CO_2 loading also affect the formation of calcium carbonate, and the increase in pH leads to an acceleration of calcium carbonate nucleation and crystal growth [32]. Crystal type and morphology have direct effects on the properties and application range of calcium carbonate. Notably, the impurity ions have an important effect on the properties of nanoscale calcium carbonate, leading to the difference between the metal ion added system and the $CaCl_2$ system of nanoscale calcium carbonate.

Korchef [33] found that Fe^{3+} hindered the nucleation of calcium carbonate under relatively low unsaturated solution conditions. Konrad *et al*. [34] reported that the different ACC (amorphous calcium carbonate) transformation mechanisms and the sequences of minerals formed were controlled by the Mg^{2+} concentration. Goncharuk *et al*. [35] investigated that the $FeCO_3$ crystals and $MnCO_3$ crystals noticeably promoted the crystallization of calcium carbonate through electrostatic action. Luo *et al*. [15], Korkut *et al*. [16], and Chang *et al*. [23] studied the preparation of calcium carbonate from waste liquids containing calcium from the ammonia steaming industry, soda ash industry, and marble waste, respectively. These studies on the preparation of nanoscale calcium carbonate from calcium-containing wastewater offered new perspectives on the efficient use of fluorite acid leaching.

The purification of fluorite was conducted in the present study to enhance the grade of fluorite concentrates by the acid leaching–flotation process, and nanoscale calcium carbonate was prepared from the acid leach solution. The leaching tests and flotation tests were performed to investigate the best beneficiation conditions for the production of high-purity fluorite concentrates. Furthermore, the morphology and crystallization of nanoscale calcium carbonate under different conditions were studied by taking the Ca^{2+}-containing leaching solution as the raw material. Nanoscale calcium carbonate with uniform particle size and excellent properties was prepared by the double decomposition method. Metal ions were added to simulate the influence of different impurity ions on the preparation of calcium carbonate, after which the main reasons for the change of the properties in nanoscale calcium carbonate were explored. Thus, an innovative way to utilize low-grade fluorite is proposed in the current study. This approach not only realized the clean treatment of mineral processing waste liquid but also saved the raw materials required (e.g., limestone) for the synthesis of nanoscale calcium carbonate. It is also conducive to the efficient and clean utilization of waste resources.

2. Experimental

2.1. Material and reagents

The low-grade fluorite used in the experiment was taken from Hunan Nonferrous Chenzhou Fluoride Chemical Co., Ltd. This material was analyzed by mineral liberation analyzer (MLA) and X-ray diffraction (XRD). The resulting XRD patterns and chemical composition are shown in Fig. 1 and Table 1, respectively.

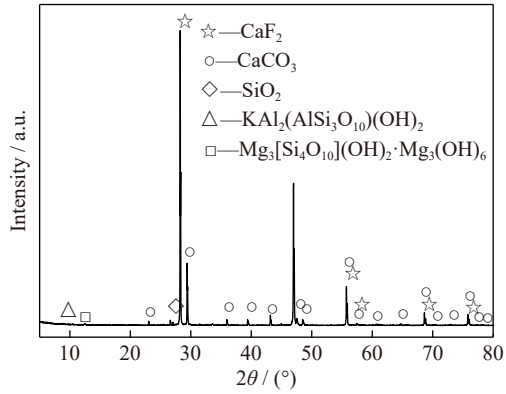

Fig. 1. X-ray diffraction pattern of raw ore.

Table 1. Chemical composition of raw ore wt%

Fluorite (CaF_2)	Muscovite ($KAl_2(AlSi_3O)(OH)_2$)	Orthoclase ($K[AlSi_3O_8]$)	Calcite ($CaCO_3$)	Quartz (SiO_2)	Chlorite ($Mg_3[Si_4O_{10}](OH)_2 \cdot Mg_3(OH)_6$)	Hedenbergite ($CaFe[Si_2O_6]$)	Other
72.88	0.99	0.50	15.01	0.95	1.09	0.81	7.77

Calcium chloride ($CaCl_2$), ammonium carbonate ($(NH_4)_2CO_3$), sodium carbonate (Na_2CO_3), citric acid ($C_6H_8O_7$), manganese chloride ($MnCl_2$), magnesium chloride ($MgCl_2$), and ferric chloride ($FeCl_3$) were all analytical-grade. Deionized water with a resistivity of >18 MΩ·cm^{-1} was used throughout the pure-material flotation experiments.

2.2. Acid leaching test

At 25°C, 100 g mineral was added into the beaker with a magnetic stirrer, after which different volumes of HCl (varied according to the liquid–solid ratio) was uniformly added into the beaker for leaching. After the reaction, the solid–li-

quid mixture was filtered and separated, and then the solid and liquid products were weighed, sampled, and analyzed individually. The experiment was repeated three times, and the average values were obtained.

2.3. Flotation test

As shown in Fig. 2, 500 g of leaching residue was added into a 1.0-L single tank flotation machine for each test. After pulp adjustment for 3 min, the pH regulator, depressant, and collector were sequentially added to the flotation cell at intervals of 3 min, and then flotation was carried out. The speed of the flotation machine was 1992 r·min^{-1}, and the speed of the scraper was 15 min^{-1}. The froth products were collected by an automatic froth scraper device, after which the products were dried, weighed, sampled, and tested before the recovery was calculated.

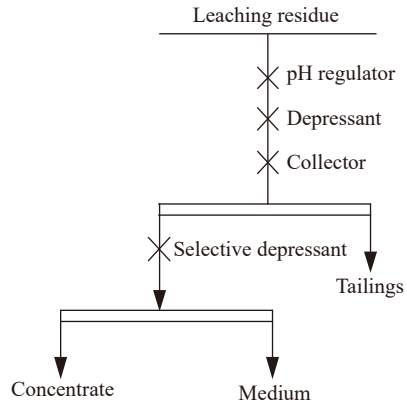

Fig. 2. Process flow diagram of flotation test.

2.4. Preparation test

About 50 mL the leached solution or $CaCl_2$ solution was measured, and the crystal regulator was added according to a certain mass fraction (the mass percentage of the crystal regulator to the theoretical $CaCO_3$). Then, 50 mL $(NH_4)_2CO_3$ solution at the same concentration as $CaCl_2$ was slowly added to the $CaCl_2$ solution using a peristaltic pump. After measuring the reactions at different reaction temperatures and stirring speeds, the calcium carbonate emulsion was filtered and washed, and the filter cake was dried at 60°C for 12 h until powdered white samples were obtained for further testing.

2.5. Measurements of properties

The ion content in the leaching solution was measured by SPECTRO BLUE SOP full-spectrum direct-reading plasma spectrometer (Inductively coupled plasma, ICP) according to GB/T 23942—2009. X-ray spectra were obtained by XRD analysis to determine the composition, component phase, internal atomic structure, and content of minerals. The cell size was calculated according to XRD data using Scherrer's formula, as shown in Eq. (1), and the contents of vaterite and calcite were estimated from XRD data using Eq. (2) [15,36]. The crystal composition of the product was analyzed by Fourier-transform infrared spectrometer (FTIR), model IR-Affinity-1, in which the measurement steps included powder tablet sampling, blank background collection, sample insert and analysis, and data preservation. The micromorphology of the product was examined using scanning electron microscopy (SEM, model JSM-6480A), in which the samples were sprayed with gold for 15–20 min before testing; the test conditions were magnified 5–300000 times, the working voltage was 2 kV, and the working distance was 10 mm. The mineral composition was measured using an MLA (MLA650). The particle size of the product was tested using a laser particle size analyzer (MASTERSIZE2000), in which the refractive index of the test sample was set at 1.572, and the background of the sample was determined with water. Then, the dispersed sample was added, and the particle size was determined after the concentration stabilized.

$$D = K\gamma/(B\cos\theta) \tag{1}$$

where K is Scherrer constant, D is the average thickness of grain perpendicular to crystal plane, B is the width of half-peak height or integral width of measured sample diffraction peak, θ is Bragg angle, and γ is X-ray wavelength (1.54056 Å).

$$f_v = 7.691I_{110v}/(7.691I_{110v} + I_{104c});\ f_c = 1 - f_v \tag{2}$$

where I_{104c} is the diffraction intensity of the calcite (104), I_{110v} is the diffraction intensity of vaterite (110), and f_v and f_c are the vaterite and calcite contents in the precipitates, respectively.

3. Results and discussion

3.1. Acid leaching test

Hydrochloric acid was used as the leaching agent during the acid leaching test, in which HCl reacted with calcite gangue to remove calcite and further dissociate fluorite minerals. The reaction principle is shown in Eq. (3). To explore the optimum conditions for acid leaching, the impacts of the dosage of HCl, leaching liquid–solid ratio, and leaching time on the leaching effect were investigated. The grade and recovery rate of leaching slag are shown in Fig. 3. As can be seen, with the increase of the dosage of HCl, fluorite grade increased significantly and then leveled off, after which the recovery of fluorite decreased slightly. The grade and recovery of fluorite increased along with the rise in the liquid–solid ratio before remaining constant. The grade and recovery of fluorite initially increased and then marginally decreased as the leaching time was extended. According to the acid leaching condition experiment, considering fluorite grade and recovery, the optimum conditions for acid leaching are as follows: liquid–solid ratio of 2:1, HCl dosage of 0.3 mol, and leaching time of 2 h. Under these conditions, fluorite grade increased from 72.56wt% to 87.94wt%, with a recovery rate of 97.63%. The results showed that acid leaching mainly dissolved most of the calcite in the fluorite and further dissociated other gangues that were connected to fluorite via calcite, which was conducive to the subsequent

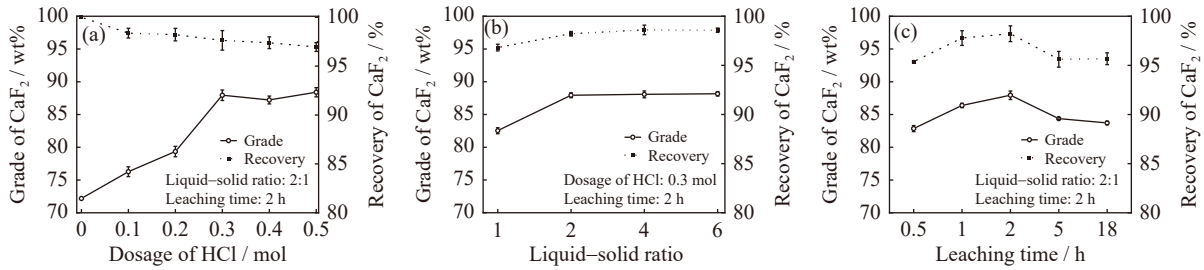

Fig. 3. Fluorite grade and recovery of leached slag under different leaching conditions: (a) dosage of HCl; (b) liquid–solid ratio; (c) leaching time.

flotation operation.

$$2HCl + CaCO_3 = CaCl_2 + H_2O + CO_2 \quad (3)$$

3.2. Flotation test

The flotation experiments were conducted using leaching slag as raw material. In the flotation process, sodium carbonate, HS, water glass, and acidized water glass was used as pH regulator, collector, coarse inhibitor, and selecting inhibitor, respectively. Both the reagent system and the physical and chemical variables have an important effect on flotation [37]. The optimum flotation conditions were pH value of 11, collector dosing of 300 $g \cdot t^{-1}$, water glass dosing of 2000 $g \cdot t^{-1}$, and 100 $g \cdot t^{-1}$ for acidized water glass through the experimental conditions. The flow chart of the acid leaching–flotation process is shown in Fig. 4. Under these conditions, the grade of CaF_2 and recovery of different samples are shown in Table 2. Without acid leaching but under the same conditions, the grade and recovery of the flotation sample are shown in Table 3. A comparison of the two processes revealed both the acid leaching and the flotation processes effectively improved the grade of fluorite more efficiently than other methods. Furthermore, the grade of fluorite increased from 87.94wt% to 97.26wt% after the acid leaching–flotation separation.

3.3. Preparation of nanoscale calcium carbonate from leaching solution

3.3.1. Process condition test

The pH of the leaching solution was adjusted to 7 by adding $Ca(OH)_2$; under neutral conditions (pH = 7), most of the metal ions formed hydroxide precipitates and were removed by filtration. In this way, we obtained a preliminary impurity removal leaching solution, which can be used to

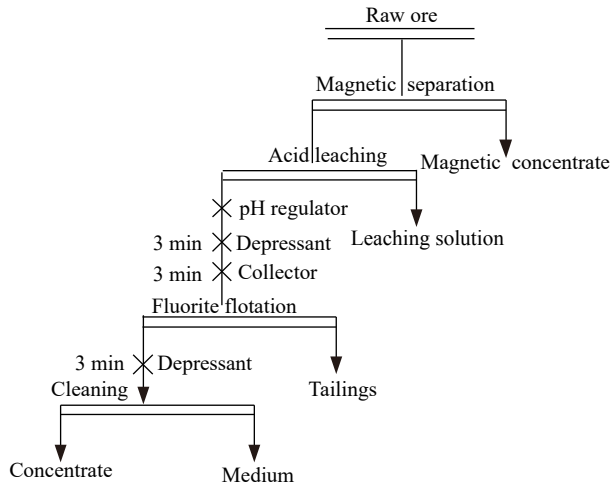

Fig. 4. Proces flow chart of acid leaching–flotation.

Table 2. Grade and recovery of the products in the acid leaching–flotation process

Sample	Yield / %	Grade of CaF_2 / wt%	Recovery of CaF_2 / %
Raw ore	100.00	72.18	100.00
Magnetic concentrate	1.56	48.00	1.04
Magnetic tailings	98.44	72.56	98.96
Leaching residue	80.13	87.94	97.63
Leaching solution	18.31	5.24	1.33
Flotation concentrate	55.08	97.26	74.22
Flotation middling	8.91	68.19	8.42
Flotation tailings	16.14	67.02	14.99

Table 3. Grade and recovery of the products in the flotation process

Sample	Yield / %	Grade of CaF_2 / wt%	Recovery of CaF_2 / %
Raw ore	100.00	72.03	100.00
Magnetic concentrate	1.56	48.00	1.04
Magnetic tailings	98.44	72.41	98.96
Flotation concentrate	47.64	87.28	57.73
Flotation middling	28.48	62.45	24.69
Flotation tailings	22.32	53.39	16.54

prepare nanoscale calcium carbonate. Next, experiments on the process conditions were conducted to prepare nanoscale calcium carbonate products with uniform crystal shapes and excellent properties. The experiments with Ca^{2+} concentration (c), temperature (T), and titration rate of $(NH_4)_2CO_3$ (V) were studied, respectively. The XRD spectra of nanoscale calcium carbonate of different concentration tests are shown in Fig. 5. The cell size and relative contents of calcite and vaterite were calculated by Eqs. (1) and (2) according to XRD data, respectively. The summary of crystal type and size changes is shown in Table 4, and the SEM images of nanoscale calcium carbonate are shown in Fig. 6.

According to the results shown in Fig. 5(a) and Table 4, when the concentrations of the reactant were 0.25 mol·L^{-1} and 0.5 mol·L^{-1} nanoscale calcium carbonate was calcite (100wt%); when it rose to 1 mol·L^{-1}, nanoscale calcium carbonate was calcite mixed with vaterite (20wt% calcite and 80wt% vaterite); and when it further increased to 2 mol·L^{-1}, the nanoscale calcium carbonate was vaterite (100wt%). These results can also be found by comparing the SEM image of Fig. 6(a) and 6(b); that is, when the concentration increased from 0.5 to 1 mol·L^{-1}, the morphology of nanoscale calcium carbonate changed from calcite type to mixed type. The increasing amount of concentration was conducive to the conversion of calcite to vaterite. In particular, with the increase in reaction concentration, the high relative content of ions in the solution promoted the formation of vaterite; therefore, the higher the reaction concentration, the easier the process of converting nanoscale calcium carbonate into vaterite [15].

According to the size changes in Table 4, the cell size of nanoscale calcium carbonate decreased with the increasing concentration, but the average particle size increased due to the formation of cells at such high concentrations. In particular, when the concentration is high, the cells form rapidly, and the growth time of cells becomes shorter, resulting in a decrease in cell size. However, this is more likely to agglomerate at a high concentration, resulting in an increase in the product's particle size. Therefore, lower concentration was more conducive to the formation of calcite-type nanoscale calcium carbonate with lower particle size, uniform size, and low degree of aggregation.

As the temperature increased, the crystalline form of nanoscale calcium carbonate transformed from calcite to vaterite. According to the XRD spectra of Fig. 5(b), when the reaction temperature was 25°C, the crystalline form of nanoscale calcium carbonate was 100wt% calcite, and when the temperature rose to 80°C, nanoscale calcium carbonate was a mixture of calcite and vaterite (65wt% calcite and 35wt% vaterite), as shown in the SEM images of Fig. 6(c), in which some vaterites were formed on the surface of calcite at 80°C. The saturation required for the nucleation of calcium carbonate crystals was in the following descending order: calcite > vaterite > aragonite. With the increase in temperature, the sat-

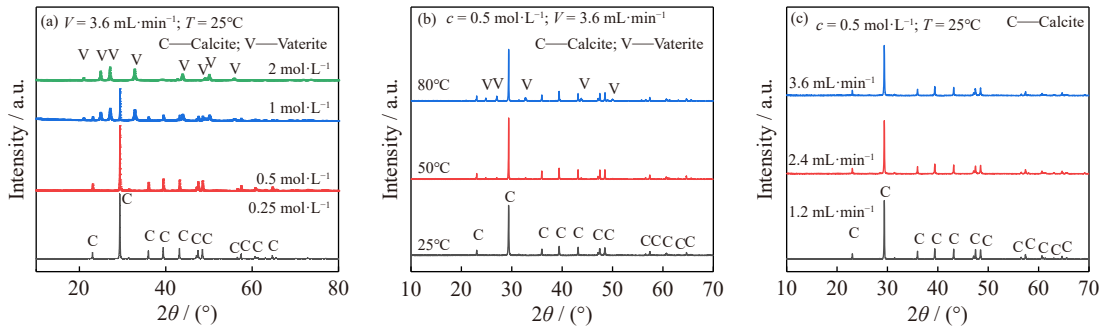

Fig. 5. X-ray diffraction spectra of nanoscale calcium carbonate prepared at different conditions: (a) at Ca^{2+} different concentrations; (b) at different temperatures; (c) at different titration rates.

Table 4. Changes in size and crystal type of different conditions

Condition			Product			
Ca^{2+} Concentration / (mol·L^{-1})	Temperature / °C	Titration rates / (mL·min^{-1})	Relative content of calcite / wt%	Relative content of vaterite / wt%	Cell size / nm	Particle size / μm
0.25	25	3.6	100	0	208.1 ± 1.3	2.535 ± 0.058
0.5	25	3.6	100	0	138.2 ± 0.7	2.667 ± 0.032
1	25	3.6	20	80	46.3 ± 0.3	4.538 ± 0.063
2	25	3.6	0	100	34.5 ± 0.2	6.225 ± 0.046
0.5	25	3.6	100	0	138.2 ± 0.7	2.667 ± 0.032
0.5	50	3.6	88	12	210.1 ± 0.8	12.155 ± 0.089
0.5	80	3.6	65	35	278.2 ± 0.9	33.333 ± 0.120
0.5	25	1.2	100	0	267.8 ± 1.0	18.540 ± 0.098
0.5	25	2.4	100	0	195.8 ± 1.0	8.186 ± 0.054
0.5	25	3.6	100	0	138.2 ± 0.8	2.667 ± 0.032

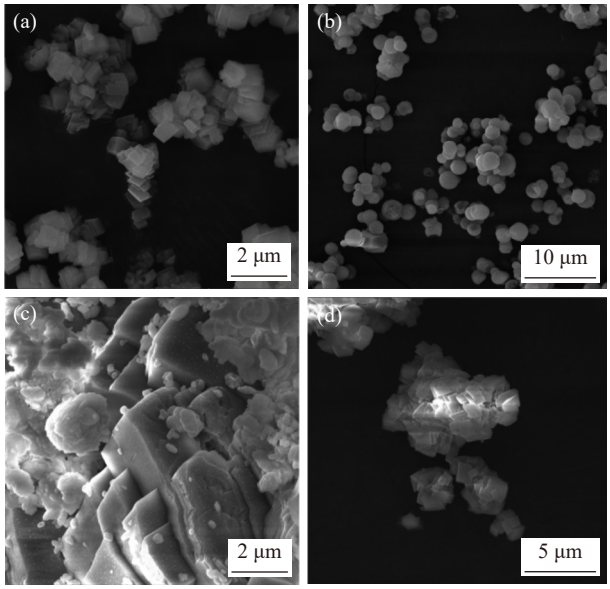

Fig. 6. Scanning electron microscopy images of nanoscale calcium carbonate prepared at different concentrations: (a) c = 0.5 mol·L^{-1}, T = 25°C, and V = 3.6 mL·min^{-1}; (b) c = 1 mol·L^{-1}, T = 25°C, and V = 3.6 mL·min^{-1}; (c) c = 0.5 mol·L^{-1}, T = 80°C, and V = 3.6 mL·min^{-1}; (d) c = 0.5 mol·L^{-1}, T = 25°C, and V = 1.2 mL·min^{-1}.

uration of the solution decreased. Therefore, elevated and low temperatures favored vaterite and calcite, respectively.

Furthermore, the particle size and cell size of nanoscale calcium carbonate increased with increasing temperature; in particular, the particle sizes were 2.667 μm at 25°C and 33.333 μm at 80°C. This means that the higher the temperature, the more favorable the growth of crystals; furthermore, the obtained calcium carbonate particle size also increased with the increase in temperature [38]. As the temperature increased, the nucleation of calcium carbonate crystals was accelerated, thus facilitating their aggregation into irregular particles. According to the comparison of the SEM images (a) and (c) in Fig. 6, the morphology of calcium carbonate was irregular, and the crystal shape fluctuated when the temperature increased to 80°C. Therefore, 25°C can be considered the optimal condition in the temperature experiment, which can prepare nanoscale calcium carbonate products with small particle size (2.667 μm) and uniform crystal (calcite type).

Meanwhile, the titration rate had no obvious effect on the crystal type of nanoscale calcium carbonate products. In fact, the nanoscale calcium carbonates all are calcite according to the XRD spectra shown in Fig. 5(c). From the SEM images of Fig. 6(a) and (d), we can see that the particle size of nanometer calcium carbonate with a titration rate of 1.2 mL·min^{-1} is much larger than that of 3.6 mL·min^{-1}. At the titration rates of 3.6 and 1.2 mL·min^{-1}, the particle sizes of nanoscale calcium carbonate were 2.667 and 18.540 μm, respectively. The particle size of the product decreasesd with the increase in titration rate. This is because the smaller the titration rate is, the longer the reaction time is, and the cell size of the product gradually increases with the increase of the reaction time. Thus, the particle size of nanoscale $CaCO_3$ decreased with the increase of the droplet acceleration of the $CaCl_2$ solution.

3.3.2. Crystal regulator test

Next, citric acid was used as a crystal regulator in the experiments. The XRD and FTIR spectra of nanoscale calcium carbonate prepared by adding citric acid at different concentrations are shown in Fig. 7. The SEM images of nanoscale calcium carbonate with a citric acid dosage of 5wt% are shown in Fig. 8, and the changes in crystal type and particle size of nanoscale calcium carbonate are shown in Table 5.

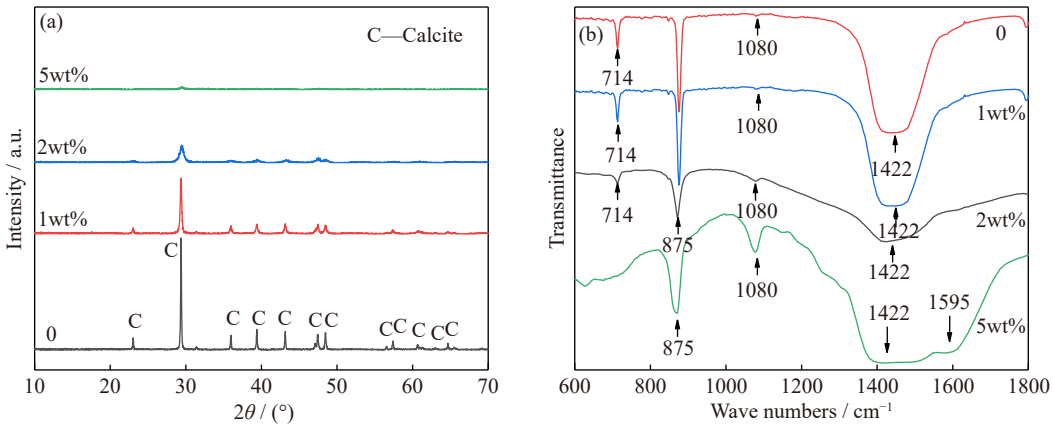

Fig. 7. (a) X-ray diffraction spectra and (b) Fourier transform infrared spectra of nanoscale calcium carbonate prepared at different citric acid dosages.

According to the XRD spectra of Fig. 7(a), with the increase of citric acid, the characteristic peak of calcite gradually weakened and finally became the characteristic peak of calcite amorphous. FTIR was used as the further characterization method, and the resulting FTIR spectra in Fig. 7(b) showed that 714, 875, 1080, and 1422 cm^{-1} were the characteristic peaks of calcite when the mass fractions of citric acid were 0, 1%, 2%, and 5% [39], and with the increase in citric acid concentration, the characteristic peak of calcite centered on 714 cm^{-1} weakened continuously. When the mass fraction of citric acid was 5%, the peaks at other locations were almost constant but lacked a distinctive vibration peak at 714 cm^{-1}. Furthermore, an additional shoulder appeared near 1422 cm^{-1}, which was a typical characteristic peak of

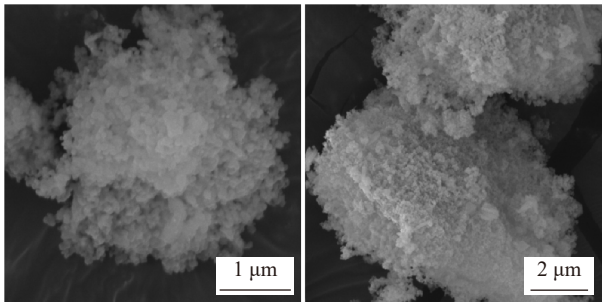

Fig. 8. Scanning electron microscopy spectrum of nanoscale calcium carbonate with a citric acid dosage of 5wt%.

amorphous calcium carbonate [40]. Thus, it was once again proved that the nanoscale calcium carbonate was amorphous when the concentration of citric acid was 5wt%.

The SEM images of amorphous calcium carbonate at 5wt% citrate dosage are shown in Fig. 8. Citric acid promoted the conversion of calcite-type nanoscale calcium carbonate to amorphous. Citrate ions can be strongly adsorbed on the surface of $CaCO_3$ due to the presence of three negatively charged polar carboxyl groups, thus reducing its surface energy and making $CaCO_3$ stable in amorphous form [39]. Amorphous calcium carbonate is a preferred material for pharmaceutical and medical applications [41]. At the same time, our results showed that the crystal growth process was inhibited, the particle size was reduced, and the nanoscale aggregates were formed. As shown in Table 5, calcite with a particle size of 1.823 μm and cell size of 11.0 nm was prepared when the mass fraction of citric acid was 2%, and amorphous nanoscale calcium carbonate with an average particle size of 1.511 μm was prepared when the mass fraction of citric acid was 5%. Thus, by adjusting the dosage of citric acid, the particle size of nanoscale calcium carbonate can be decreased.

Table 5. Changes in size and crystal types of different citric acid dosages

Citric acid dosage / wt%	Crystal type	Cell size / nm	Particle size / μm
0	Calcite	138.2	2.667
1	Calcite	63.3	2.322
2	Calcite	11.0	1.823
5	Amorphous		1.511

3.4. Comparison of the leaching solution and $CaCl_2$ systems

Impurity ions in the leaching solution may have an important role in the preparation of nano-calcium carbonates. Thus, the nano-calcium carbonates prepared by the leaching liquid system and the $CaCl_2$ system under the same conditions were compared to further explore the formation mechanism of nano-calcium carbonate in the leaching solution and explore the role of impurity ions. In particular, the XRD spectra, SEM spectra, and size of nanoscale calcium carbonate under the $CaCl_2$ system and the leached liquid systems were compared, as shown in Figs. 9 and 10, and Table 6. Under the same conditions, the calcite-type calcium carbonates with a particle size of 2.667 μm were prepared by the leaching liquid, and the calcium carbonates (30wt% calcite and 70wt% vaterite) with a particle size of 9.491 μm were prepared by $CaCl_2$. The results showed that nanoscale calcium carbonate products in the leaching liquid system more likely transformed to calcite type, and the cell size and average particle size of nanoscale calcium carbonate products decreased compared with those produced using the $CaCl_2$ system.

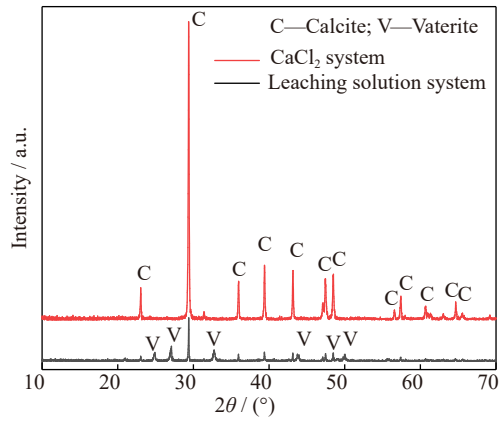

Fig. 9. X-ray diffraction spectra of nanoscale calcium carbonates prepared at different systems.

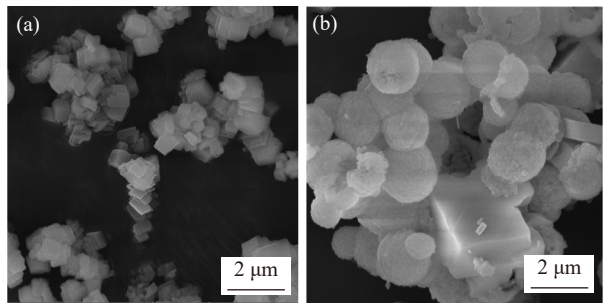

Fig. 10. Scanning electron microscopy spectra of nanoscale calcium carbonates prepared at different systems: (a) leaching solution system; (b) $CaCl_2$ system.

According to ICP detection (Table 7), the impurity ions with high concentrations in the leaching solution included Mn^{2+}, Mg^{2+}, and Fe^{3+}. To explore the reason for the change in the nanoscale calcium carbonate products of the leaching liquid, the main ions in the leaching solution were introduced

Table 6. Comparison of the changes in size and crystal type between the leaching solution and $CaCl_2$ systems

System	Relative content of calcite / wt%	Relative content of vaterite / wt%	Cell size / nm	Particle size / μm
Leaching liquid system	100	0	138.2	2.667
$CaCl_2$ system	30	70	408.0	9.491

and compared. Under the same conditions, $MgCl_2$, $MnCl_2$, and $FeCl_3$ were added to the $CaCl_2$ solution with mass fractions (relative to the mass of $CaCl_2$) of 0.9%, 0.33%, and 0.08%, respectively, to prepare nanoscale calcium carbonates. The test results of nanoscale calcium carbonate are shown in Fig. 11 and Table 8.

Table 7. Main elemental composition of the leaching solution mg·L^{-1}

Ca	Fe	Mn	Ba	Mg	Al
36004	28.6	321.7	0.8	119.4	0.5

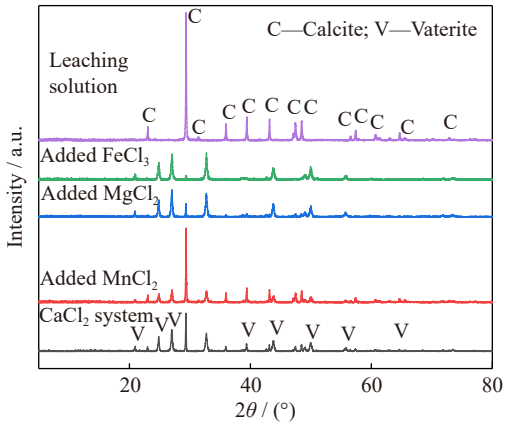

Fig. 11. X-ray diffraction spectra of nanoscale calcium carbonate prepared at different systems.

The solubilities of $MgCO_3$ [42], $CaCO_3$ [43], $FeCO_3$ [44], and $MnCO_3$ [42,45] decreased sequentially under the condition of pH 7 at 25°C [46]. The XRD spectra showed that Mn^{2+} promoted the transformation of nanoscale calcium carbonate from vaterite to calcite because Mn^{2+} was incorporated into calcite lattice to form a $CaCO_3$–$MnCO_3$ solid solution [45,47], in which Mn^{2+} entered into the calcium carbonate lattice to form groups. This resulted in the formation of a layer of manganese-based compounds on the surface of vaterite and a barrier between the species of vaterite, which prevented the aggregation of spherical particles and promoted the formation of cubic calcite [45,48]. Mg^{2+} and Fe^{3+} inhibited the conversion of nanoscale calcium carbonate from vaterite to calcite. In particular, Mg^{2+} and Fe^{3+} entered the calcite lattice and replaced part of Ca^{2+} in calcite, resulting in lattice distortion and difficult formation of calcite nucleus [35]. $MgCO_3$ has a high solubility, and its entry into the $CaCO_3$ lattice resulted in the change of transformation pathway of amorphous calcium carbonate to calcite [42]. The different transformation mechanisms of amorphous calcium carbonate and the resulting crystal forms are controlled by the Mg^{2+} concentration in the reaction solution, in which the higher the Mg^{2+} concentration, the more it inhibits the calcite formation [47]. Furthermore, Fe^{3+} reacted with carbonate to form siderite ($FeCO_3$) and inhibit calcite [43]. The inhibition effectiveness of iron ions on calcium carbonate crystallization depends strongly on the solution supersaturations, where it becomes greater at lower supersaturations [33]. Mn^{2+}, Mg^{2+}, and Fe^{3+} all adsorbed on the surface of the nanoscale meter calcium carbonate and inhibited the growth of the cell, thus reducing the particle size of nanoscale calcium carbonate [30].

Compared with the products of the $CaCl_2$ system, the crystal type in the leaching solution system was mainly changed by the influence of Mn^{2+}, which may be due to the higher content of Mn^{2+} in the leaching solution than other impurity ions, resulting in a dominant influence compared with others. Our results showed that the particle size reduction was caused by the joint influence of Mn^{2+}, Mg^{2+}, and Fe^{3+}. This finding is of great significance for the preparation of nanoscale calcium carbonate from a leaching solution. Furthermore, the crystalline form of nanoscale calcium carbonate can be regulated by controlling the concentration of metal ions (Mn^{2+}, Mg^{2+}, and Fe^{3+}) in the process of removing impurities at the early stage of preparation. At the same time, the effect of metal ions on reducing the particle size can be fully maximized to prepare nanoscale calcium carbonate products with expected crystalline form and small particle size.

Table 8. Changes in size and crystal type of different ions

Added ion	Specific gravity of calcite / wt%	Specific gravity of vaterite / wt%	Cell size / nm	Particle size / μm
$CaCl_2$ system	30	70	408.0	9.491
Mn^{2+}	55	45	378.3	7.431
Mg^{2+}	10	90	403.4	8.020
Fe^{3+}	5	95	382.4	9.432
Leaching solution	100	0	138.2	2.667

4. Conclusions

Low-grade fluorite can be efficiently purified by the acid leaching–flotation process. Under the optimal process conditions, the grade of fluorite increased to 97.26wt%, and the recovery was 74.22%. A reaction concentration of 0.5 mol·L^{-1}, pH value of 7, titration rate of 3.6 mL·min^{-1}, and reaction temperature of 25°C were found to be the ideal process conditions. Calcite-type calcium carbonate nanoscale particles with cell sizes of 138.2 nm and average particle sizes of 2.667 μm were created under these processing conditions. By adding 2wt% citric acid to the leaching solution, the particle size of calcite-type nanoscale calcium carbonate was reduced to 1.823 μm. After adding 5wt% citric acid to the leaching solution, the calcite-type nanoscale calcium carbonate was transformed into an amorphous type, and the particle

size was decreased to 1.511 μm.

Due to the effects of the dissolved metal ions in the leaching solution, the nanoscale calcium carbonate generated in the leaching liquid system tended to be transformed into calcite, and its particle size was reduced when compared with the results of the $CaCl_2$ system. Moreover, Mg^{2+} and Fe^{3+} enhanced vaterite formation, whereas Mn^{2+} promoted calcite production. The preparation of nanoscale calcium carbonate products with the anticipated crystalline form and particle size was made possible by fully utilizing the action of metal ions on particle size reduction and crystal type modification.

Acknowledgements

This work was financially supported by the National Key Research Center and Development Program of the 14th Five-Year Plan, China (No. 2022YFC2905105), National Natural Science Foundation of China (Nos. 52122406 and 52004337), Hunan High-tech Industry Technology Innovation Leading Plan, China (No. 2022GK4056), Hunan Innovative Province Construction Special Project, China (No. 2020RC3001), and Hunan Postgraduate Research and Innovation Project, China (No. CX20220200).

Conflicts of Interest

All authors declare that they have no financial interests or personal relationships that could have appeared to influence the work reported in this paper.

References

[1] T.T. Basiev, M.E. Doroshenko, V.A. Konyushkin, *et al*., Fluoride optical nanoceramics, *Russ. Chem. Bull.*, 57(2008), No. 5, p. 877.

[2] W.H. Kan and V. Thangadurai, Challenges and prospects of anodes for solid oxide fuel cells (SOFCs), *Ionics*, 21(2015), No. 2, p. 301.

[3] F.A. Shah, Fluoride-containing bioactive glasses: Glass design, structure, bioactivity, cellular interactions, and recent developments, *Mater. Sci. Eng. C*, 58(2016), p. 1279.

[4] D. Němec, Fluorine in lamprophyre and lamproid rocks, *Geochim. Cosmochim. Acta*, 32(1968), No. 5, p. 523.

[5] V.A. Sadykov, M.N. Simonov, Y.N. Bespalko, *et al*., Design and characterization of nanocomposite catalysts for biofuel conversion into syngas and hydrogen in structured reactors and membranes, *Kinet. Catal.*, 60(2019), No. 5, p. 582.

[6] C.B. Shi, J.W. Cho, D.L. Zheng, and J. Li, Fluoride evaporation and crystallization behavior of CaF_2–CaO–Al_2O_3–(TiO_2) slag for electroslag remelting of Ti-containing steels, *Int. J. Miner. Metall. Mater.*, 23(2016), No. 6, p. 627.

[7] R.F. Sun, *Effect and Mechanism of Metal Ions on Calcite Inhibitors in Fluorite Flotation System* [Dissertation], Kunming University of Science and Technology, Kunming, 2022, p. 12.

[8] Z.Y. Gao, C. Wang, W. Sun, Y.S. Gao, and P.B. Kowalczuk, Froth flotation of fluorite: A review, *Adv. Colloid Interface Sci.*, 290(2021), art. No. 102382.

[9] H.P. Zhou, Z.Z. Yang, Y.B. Zhang, F.X. Xie, and X.P. Luo, Flotation separation of smithsonite from calcite by using flaxseed gum as depressant, *Miner. Eng.*, 167(2021), art. No. 106904.

[10] J.W. Huang, Q.W. Zhang, H.C. Li, and C. Wang, Difficulties and recent achievements in flotation separation of fluorite from calcite—An overview, *Minerals*, 12(2022), No. 8, art. No. 957.

[11] R.L. Wang, H.S. Han, W. Sun, A.V. Nguyen, W.J. Sun, and Z. Wei, Hydrophobic behavior of fluorite surface in strongly alkaline solution and its application in flotation, *Colloids Surf. A: Physicochem. Eng. Aspects*, 609(2021), art. No. 125661.

[12] D.Q. Wang, D. Liu, Y.B. Mao, R.F. Sun, R.T. Liu, and S.M. Wen, Effect of fluoride ion on the separation of fluorite from calcite using flotation with acidified water glass, *Minerals*, 11(2021), No. 11, art. No. 1203.

[13] Q.Q. Lin, G.H. Gu, H. Wang, R.F. Zhu, Y.C. Liu, and J.G. Fu, Preparation of manganese sulfate from low-grade manganese carbonate ores by sulfuric acid leaching, *Int. J. Miner. Metall. Mater.*, 23(2016), No. 5, p. 491.

[14] S.M. El-Sheikh and M.A. Rabah, Optical properties of calcium chromate 1D-nanorods synthesized at low temperature from secondary resources, *Opt. Mater.*, 37(2014), p. 235.

[15] X.P. Luo, X.W. Song, Y.W. Cao, L. Song, and X.Z. Bu, Investigation of calcium carbonate synthesized by steamed ammonia liquid waste without use of additives, *RSC Adv.*, 10(2020), No. 13, p. 7976.

[16] I. Korkut, A. Civas, and M. Bayramoglu, Effects of ultrasound and process parameters on the precipitation of $CaCO_3$ polymorphs from synthetic soda ash industry liquid waste, *Chem. Eng. Process.*, 168(2021), art. No. 108584.

[17] J.S. Han, S.Y. Jung, D.S. Kang, and Y.B. Seo, Development of flexible calcium carbonate for papermaking filler, *ACS Sustainable Chem. Eng.*, 8(2020), No. 24, p. 8994.

[18] W. Wu, X.Q. Zhang, J.F. Chen, and S.L. Shen, Synthesis of nano-$CaCO_3$ composite particles and their application, *J. Univ. Sci. Technol. Beijing*, 15(2008), No. 1, p. 67.

[19] M.L. Cao, X. Ming, K.Y. He, L. Li, and S. Shen, Effect of macro-, micro- and nano-calcium carbonate on properties of cementitious composites—A review, *Materials*, 12(2019), No. 5, p. 781.

[20] H. Lin, Y.B. Dong, and L.Y. Jiang, Preparation of calcium carbonate particles coated with titanium dioxide, *Int. J. Miner. Metall. Mater.*, 16(2009), No. 5, p. 592.

[21] X.Y. Zhou, R. Yu, J.H. Jiang, *et al*., PEEK composite resin with enhanced intumescent flame retardancy loaded with Octaphenylsilsesquioxane and nano calcium carbonate and its application in fibers, *Polym. Degrad. Stab.*, 202(2022), art. No. 110042.

[22] C.C. Zeng, H.M. Hu, X.H. Feng, K. Wang, and Q.W. Zhang, Activating $CaCO_3$ to enhance lead removal from lead-zinc solution to serve as green technology for the purification of mine tailings, *Chemosphere*, 249(2020), art. No. 126227.

[23] Y. Chang, H.J. Han, T.T. Liu, *et al*., Cell-tailored calcium carbonate particles with different crystal forms from nanoparticle to nano/microsphere, *RSC Adv.*, 10(2020), No. 70, p. 43233.

[24] L.T. Kang, M.W. Cui, F.Y. Jiang, *et al*., Nanoporous $CaCO_3$ coatings enabled uniform Zn stripping/plating for long-life zinc rechargeable aqueous batteries, *Adv. Energy Mater.*, 8(2018), No. 25, art. No. 1801090.

[25] A.S.A. Mohammed, A. Carino, A. Testino, M.R. Andalibi, and A. Cervellino, *In situ* liquid SAXS studies on the early stage of calcium carbonate formation, *Part. Part. Syst. Char.*, 36(2019), No. 6, art. No. 1800482.

[26] B. Wang, Z.H. Pan, H.G. Cheng, Z.E. Zhang, and F.Q. Cheng, A review of carbon dioxide sequestration by mineral carbonation of industrial byproduct gypsum, *J. Cleaner Prod.*, 302(2021), art. No. 126930.

[27] Y. Wei, H. Xu, S.M. Xu, *et al*., Synthesis and characterization of calcium carbonate on three kinds of microbial cells templates, *J. Cryst. Growth*, 547(2020), art. No. 125755.

[28] A. Katsman, I. Polishchuk, and B. Pokroy, On the mechanism

of calcium carbonate polymorph selection via confinement, *Faraday Discuss.*, 235(2022), p. 433.
[29] M. Ma, Y.H. Wang, X.F. Cao, W.P. Lu, and Y.C. Guo, Temperature and supersaturation as key parameters controlling the spontaneous precipitation of calcium carbonate with distinct physicochemical properties from pure aqueous solutions, *Cryst. Growth Des.*, 19(2019), No. 12, p. 6972.
[30] J. Wang, J.Z. Song, Z.Y. Ji, *et al*., The preparation of calcium carbonate with different morphologies under the effect of alkanolamide 6502, *Colloids Surf., A*, 588(2020), art. No. 124392.
[31] X.H. Mei, Q. Zhao, Y.M. Li, *et al*., Phase transition and morphology evolution of precipitated calcium carbonate (PCC) in the CO_2 mineralization process, *Fuel*, 328(2022), art. No. 125259.
[32] A. Korchef and M. Touaibi, Effect of pH and temperature on calcium carbonate precipitation by CO_2 removal from iron-rich water, *Water Environ. J.*, 34(2020), No. 3, p. 331.
[33] A. Korchef, Effect of iron ions on the crystal growth kinetics and microstructure of calcium carbonate, *Cryst. Growth Des.*, 19(2019), No. 12, p. 6893.
[34] F. Konrad, B. Purgstaller, F. Gallien, V. Mavromatis, P. Gane, and M. Dietzel, Influence of aqueous Mg concentration on the transformation of amorphous calcium carbonate, *J. Cryst. Growth*, 498(2018), p. 381.
[35] V.V. Goncharuk, V.A. Bagrii, S.Y. Bashtan, R.D. Chebotareva, and A.V. Nanieva, Crystalization of calcium carbonate in magnetized water in the presence of ions of iron and manganese, *J. Water Chem. Technol.*, 33(2011), No. 3, p. 160.
[36] C.G. Kontoyannis and N.V. Vagenas, Calcium carbonate phase analysis using XRD and FT-Raman spectroscopy, *Analyst*, 125(2000), No. 2, p. 251.
[37] A. Gomez-Flores, G.W. Heyes, S. Ilyas, and H. Kim, Prediction of grade and recovery in flotation from physicochemical and operational aspects using machine learning models, *Miner. Eng.*, 183(2022), art. No. 107627.
[38] R. Ševčík, M. Pérez-Estébanez, A. Viani, P. Šašek, and P. Mácová, Characterization of vaterite synthesized at various temperatures and stirring velocities without use of additives, *Powder Technol.*, 284(2015), p. 265.
[39] X. Xia, J.W. Chen, J. Shen, D. Huang, P.Z. Duan, and G.H. Zou, Synthesis of hollow structural hydroxyapatite with different morphologies using calcium carbonate as hard template, *Adv. Powder Technol.*, 29(2018), No. 7, p. 1562.
[40] N. Mehta, J. Gaëtan, P. Giura, T. Azaïs, and K. Benzerara, Detection of biogenic amorphous calcium carbonate (ACC) formed by bacteria using FTIR spectroscopy, *Spectrochim. Acta, Part A*, 278(2022), art. No. 121262.
[41] J.T. Avaro, C. Ruiz-Agudo, E. Landwehr, K. Hauser, and D. Gebauer, Impurity-free amorphous calcium carbonate, a preferential material for pharmaceutical and medical applications, *Eur. J. Mineral.*, 31(2019), No. 2, p. 231.
[42] J.R. Goldsmith and H.C. Heard, Subsolidus phase relations in the system $CaCO_3$–$MgCO_3$, *J. Geol.*, 69(1961), No. 1, p. 45.
[43] T.Y. Chen, S. Honarparvar, D. Reible, and C.C. Chen, Thermodynamic modeling of calcium carbonate scale precipitation: Aqueous Na^+–Ca^{2+}–Cl^-–HCO_3^-–CO_3^{2-}–CO_2 system, *Fluid Phase Equilib.*, 552(2022), art. No. 113263.
[44] P. Bénézeth, J.L. Dandurand, and J.C. Harrichoury, Solubility product of siderite ($FeCO_3$) as a function of temperature (25–250°C), *Chem. Geol.*, 265(2009), No. 1-2, p. 3.
[45] K.S. Johnson, Solubility of rhodochrosite ($MnCO_3$) in water and seawater, *Geochim. Cosmochim. Acta*, 46(1982), No. 10, p. 1805.
[46] J.A. Dean, *Lange's Handbook of Chemistry*, McGraw-Hill Professional Publishing, New York, 1985.
[47] J.V. Mills, H.A. Barnhart, D.J. DePaolo, and L.N. Lammers, New insights into Mn^{2+} and Mg^{2+} inhibition of calcite growth, *Geochim. Cosmochim. Acta*, 334(2022), p. 338.
[48] E.J. Zeller and J.L. Wray, Factors influencing precipitation of calcium carbonate, *AAPG Bull.*, 40(1956), No. 1, p. 140.